JACS
JOURNAL OF THE AMERICAN CHEMICAL SOCIETY

Communication

pubs.acs.org/JACS

Improving the Electrode Performance of Ge through Ge@C Core–Shell Nanoparticles and Graphene Networks

Ding-Jiang Xue, Sen Xin, Yang Yan, Ke-Cheng Jiang, Ya-Xia Yin, Yu-Guo Guo,* and Li-Jun Wan*

Key Laboratory of Molecular Nanostructure and Nanotechnology and Beijing National Laboratory for Molecular Sciences, Institute of Chemistry, Chinese Academy of Sciences (CAS), Beijing 100190, P. R. China

Supporting Information

ABSTRACT: Germanium is a promising high-capacity anode material for lithium ion batteries, but it usually exhibits poor cycling stability because of its huge volume variation during the lithium uptake and release process. A double protection strategy to improve the electrode performance of Ge through the use of Ge@C core–shell nanostructures and reduced graphene oxide (RGO) networks has been developed. The as-synthesized Ge@C/RGO nanocomposite showed excellent cycling performance and rate capability in comparison with Ge@C nanoparticles when used as an anode material for Li ion batteries, which can be attributed to the electronically conductive and elastic RGO networks in addition to the carbon shells and small particle sizes of Ge. The strategy is simple yet very effective, and because of its versatility, it may be extended to other high-capacity electrode materials with large volume variations and low electrical conductivities.

Rechargeable lithium ion batteries are essential for portable electronics, electric vehicles, and the storage of renewable energy.[1,2] Because of the rapid development of such applications, Li ion batteries with high energy density and long cycle life are required. High-energy-density batteries can be achieved by utilizing electrode materials with higher specific capacities than current commercial ones.[3,4] Compared with the graphite anode, which has a theoretical specific capacity of 372 mA h g^{-1}, Li alloys of group IV materials have attracted increasing attention as potential high-capacity anode materials. Especially, silicon and germanium are two stars because of their high theoretical capacities of 4200 and 1600 mA h g^{-1}, respectively.[5] Though Ge has attracted less attention than Si recently because of its higher cost, the increased interest in Ge could bring about a decrease in its cost as a result of the abundance of Ge in the Earth's crust.[6] In addition, compared with Si, Ge has advantages for high-power Li ion batteries because of its intrinsic kinetic superiority. On one hand, the electrical conductivity of Ge is 10^4 times higher than that of Si because of its smaller band gap of 0.6 eV.[7] On the other hand, the Li diffusion coefficient of Ge is also 400 times higher than that of Si at room temperature.[6,8] However, the commercial application of Ge in Li ion batteries is still hindered by the poor cycle stability, similar to Si. The main reason is that during the Li uptake and release process there is a drastic volume change of the active materials that results in their pulverization and exfoliation from the current collector, leading to poor cyclability and rapidly declining capacity.[9,10] To overcome this problem, tremendous efforts have been made to design materials that can buffer the volume change, including the use of nanosized Ge particles,[11] wires, or tubes,[12−15] the synthesis of porous Ge,[16] and coating with carbon.[9,17] Among the various approaches, Ge nanoparticles (NPs) coated with carbon shells are attractive in improving the cycling performance.[9,11] On one hand, decreasing the size of Ge particles to the nanoscale can mitigate the physical strains during the Li uptake/release process, so the volume change causes less cracking and particle pulverization.[9,11] On the other hand, the carbon shell with moderate kinetic properties toward Li ion and electron transport also plays a structural buffering role in minimizing the mechanical stress induced by the volume change of Ge.[11] This strategy leads to enhanced capacity in initial several cycles but is naturally not meant to achieve long cycle life and high power demands because of the unavoidable agglomeration of small NPs.[18] It is still a big challenge to enhance both the cyclability and rate capability of Ge anode materials.

Graphene is a good candidate to host active NPs for Li ion batteries because of its high electrical conductivity, large surface area, flexibility, and chemical stability. Recently, various hybrid nanostructures containing graphene nanosheets have been designed as electrode materials.[19−27] In comparison with other carbon matrixes such as graphite, carbon black, and carbon nanotubes, graphene sheets afford good dispersion of the NPs and guarantee a high electrical conductivity of the overall electrode, which is good for the purpose of high rates.[19−27] Nevertheless, the NPs may still undergo successive agglomeration during the Li uptake/release process, leading to capacity fading, if the active NPs in the nanocomposites are directly exposed to the electrolyte.[19,24,28−30] To address this problem, core–shell NPs might be helpful.[9,11,31] However, according to our knowledge, there has been no report on the combination of a Ge@C core–shell structure and the use of graphene.

One of the most promising strategies for tackling the aggregation problem of electrode materials is to confine them within individual carbon shells and then to distribute the wrapped NPs within carbon shells onto the surface of graphene,[25] thus forming mixed conducting 3D networks, which have been shown to be highly efficient for Li storage.[28,30,32] If this double protection strategy of active electrode materials could be realized, high-performance anode materials would be expected.

Herein we propose and realize a double protection strategy for improving both the cyclability and rate capability of Ge

Received: December 1, 2011
Published: January 17, 2012

   dx.doi.org/10.1021/ja211266m | J. Am. Chem.Soc. 2012, 134, 2512–2515

anodes. Ge NPs are first covered by a carbon nanocoating layer, avoiding direct exposure of the NPs to the electrolyte. Elastic reduced graphene oxide (RGO) networks are then introduced for dispersing, embedding, and electrically wiring the Ge@C core−shell NPs. The power of this concept is demonstrated by the facile synthesis of the Ge@C/RGO nanocomposite, which shows much-improved specific capacity, cycling performance, and rate capability in comparison with pristine Ge@C NPs when used as an anode material for Li ion batteries.

Figure 1 shows a schematic illustration of the synthesis route for the Ge@C/RGO nanocomposite. In a typical synthesis,

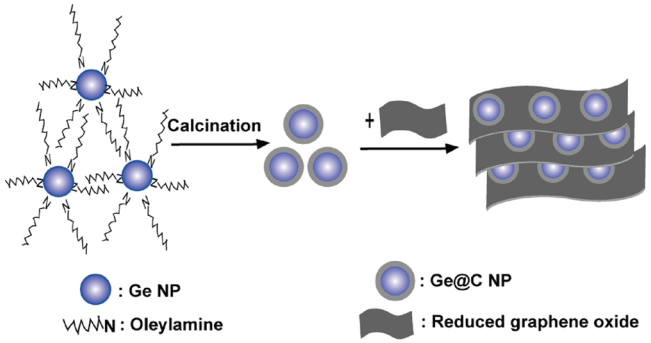

Figure 1. Schematic illustration of the synthesis route for the Ge@C/RGO nanocomposite.

Ge NPs were prepared using a solution method based on the reaction between $GeBr_2$ and oleylamine, as reported previously.[33] The as-obtained Ge NPs capped with oleylamine were then subjected to carbonization at 500 °C for 2 h under Ar containing 5% H_2 to obtain a dark powder. Graphene oxide (GO) was synthesized according to the modified Hummer's method starting from graphite powder.[34] GO was then reduced into RGO by heating at 900 °C for 2 h under Ar containing 5% H_2; details of the characterization of the as-obtained RGO have been reported previously.[23] The Ge@C/RGO nanocomposite was prepared by dispersing the two materials Ge@C and RGO (16:1 w/w) in ethanol solution and slowly drying at 50 °C. During the solvent vaporization, the Ge@C NPs were gradually deposited and embedded in the RGO networks.

Figure 2a shows the X-ray diffraction (XRD) pattern of the as-prepared Ge@C NPs, in which all of the XRD peaks are in

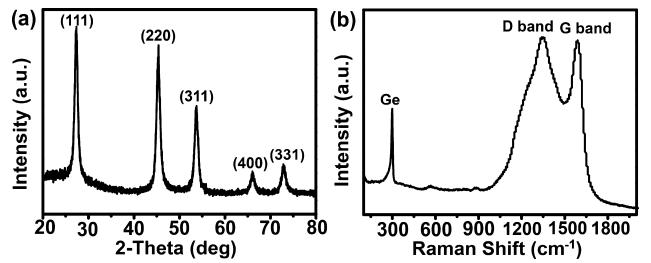

Figure 2. (a) XRD pattern and (b) Raman spectrum of the as-prepared Ge@C NPs.

good agreement with diamond cubic Ge (JCPDS card no. 04-0545). No obvious peaks corresponding to carbon are found in the XRD pattern, indicating that the carbon in the sample is not well crystallized. Raman spectroscopy was employed to confirm further the crystalline phase of Ge and the existence of carbon in the Ge@C NPs (Figure 2b). The three characteristic peaks at 298, 1346, and 1588 cm^{-1} are in good agreement with the typical Raman mode of Ge and the D band (disordered induced phonon mode) and G band (graphite band) of C, respectively. Thermogravimetric analysis (TGA), carried out in air at a heating rate of 10 °C min^{-1}, was used to determine the chemical composition of the Ge@C composite (Figure S1 in the Supporting Information). The results showed the Ge@C composite to contain ~38 wt % carbon (GeO_2 was supposed to be the final product).

The size and morphology of the Ge@C/RGO nanocomposite were characterized by transmission electron microscopy (TEM). Figure 3a,b shows typical TEM images of the Ge@C NPs, which

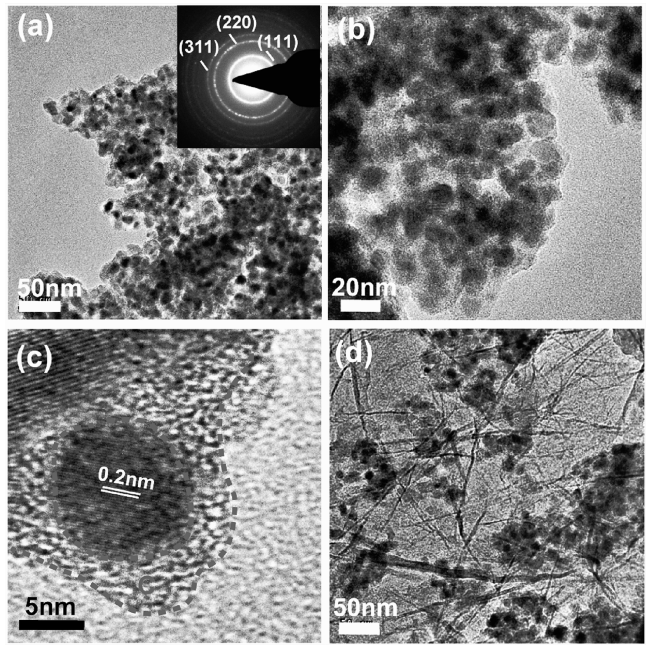

Figure 3. (a−c) TEM images and SAED pattern (inset) of the as-prepared Ge@C NPs at different magnifications. (d) TEM image of the Ge@C/RGO nanocomposite.

clearly indicate the sizes of Ge NPs wrapped within carbon shells to be 10−15 nm. The selected-area electron diffraction (SAED) pattern (Figure 3a inset) also reveals that the NPs have a diamond cubic structure. The calculated *d* spacings from the SAED pattern are 0.33, 0.2, and 0.17 nm, which match well with the *d* spacing values for the (111), (220), and (311) planes of diamond cubic Ge, respectively. Figure 3b clearly shows the marked contrast between the crystalline Ge and the carbon; the dark cores correspond to Ge NPs. The Ge NPs are well-enclosed within carbon shells. In the high-resolution TEM image (Figure 3c), crystalline planes of Ge(220) with a distance spacing of 0.2 nm can be clearly observed. It can also clearly be seen that the Ge NPs are well-covered by a carbon layer with a thickness of 2−3 nm. Figure 3d shows a TEM image of the as-prepared Ge@C/RGO nanocomposite. It can be seen that the Ge@C NPs are well-dispersed in the networks made from thin RGO nanosheets. The low aggregation of Ge@C NPs in the nanocomposites (Figure 3d) in comparison with the RGO-free Ge@C NPs (see Figure 3a,b) indicates that the RGO nanosheets play an essential role in achieving good dispersion of the Ge@C NPs.

The electrochemical performance of the Ge@C/RGO nanocomposite was tested by galvanostatic discharge−charge

dx.doi.org/10.1021/ja211266m | J. Am. Chem.Soc. 2012, 134, 2512−2515

technique. Figure 4a shows the discharge−charge voltage profiles cycled under a current density of 50 mA g^{-1} over the

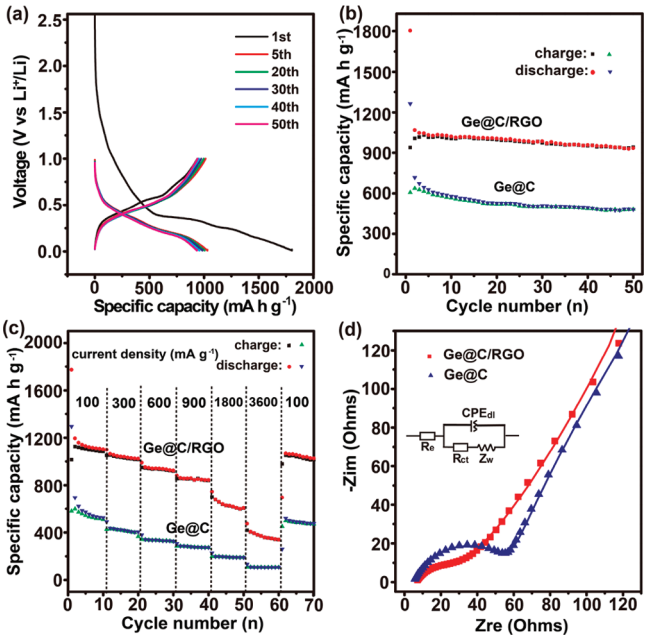

Figure 4. (a) Discharge−charge curves of Ge@C/RGO nanocomposites cycled between 0 and 1.0 V under a current density of 50 mA g^{-1}. (b) Cycling behaviors of Ge@C/RGO nanocomposites and Ge@C NPs under a current density of 50 mA g^{-1}. (c) Cycling performances of Ge@C/RGO nanocomposites and Ge@C NPs under different current densities. (d) Nyquist plots of the electrodes of Ge@C/RGO nanocomposites and Ge@C NPs.

voltage range 0−1.0 V vs Li^+/Li. The initial discharge and charge specific capacities are 1803 and 938 mA h g^{-1}, respectively, based on the total mass of the Ge@C/RGO nanocomposite. The large initial discharge capacity of the nanocomposite could be attributed to the formation of solid electrolyte interphase (SEI) films on the surface of the electrode due to electrolyte decomposition, similar to that reported in nanosized lithium alloy systems.[12] In addition, the graphene networks with high surface area may also contribute to this issue. Though a large irreversible capacity loss was observed in the first cycle, the reversibility of the capacity was significantly improved, with an average columbic efficiency of >99% for up to 50 cycles after the second cycle. The initial irreversible capacity loss could be mainly ascribed to irreversible Li insertion into the nanocomposites, in addition to the formation of SEI films on the surface of the electrode materials. This has been well-studied in carbonaceous electrodes and observed in Ge and Si electrodes.[9,12,35,36]

Pristine Ge@C NPs without RGO were also tested for comparison. As shown in Figure 4b, the Ge@C/RGO nanocomposites exhibit a higher specific capacity and better cycling stability than the pristine Ge@C NPs. After 50 cycles under a current density of 50 mA g^{-1}, the Ge@C/RGO nanocomposites still retain a reversible capacity of ~940 mA h g^{-1}, which is ~3 times higher than the theoretical capacity of graphite, whereas the Ge@C NPs only show a specific capacity lower than 490 mA h g^{-1}.

Another considerable improvement is the rate capability of the Ge@C/RGO nanocomposites in comparison with the pristine Ge@C NPs. As shown in Figure 4c, the Ge@C/RGO nanocomposites show a much higher capacity than the pristine Ge@C NPs under all investigated current densities (see Figure S2 for the discharge−charge curves). Even under the very high current density of 3600 mA g^{-1}, the Ge@C/RGO nanocomposites still exhibit a favorable specific capacity of 380 mA h g^{-1} after 50 cycles, which is still higher than the theoretical capacity of graphite, while Ge@C NPs only show a specific capacity of 100 mA h g^{-1}. Importantly, after the high-rate measurements, the specific capacities of the electrode materials cycled under 100 mA g^{-1} were able to recover to the initial reversible values, implying their good reversibility.

The much improved electrochemical performance of the Ge@C/RGO nanocomposites in comparison with pristine Ge@C NPs could be attributed to the unique properties of the proposed structural design with double protection. First, the carbon shell acts as a buffer that plays an important role in minimizing volume changes and direct contact between Ge and the electrolyte, facilitating the formation of a stable SEI, which contributes to the good cycling performance.[9,11] Second, the RGO networks, which serve as the elastic and electronically conductive substrate, afford good dispersion of the NPs and guarantee a high electrical conductivity of the overall electrode, hence realizing much improved specific capacity, cycling performance, and rate capability.

The enhanced electrical conductivity of the Ge@C/-RGO nanocomposite was confirmed by electrochemical impedance spectroscopy (EIS). Figure 4d compares the Nyquist plots for the Ge@C/RGO nanocomposites and the Ge@C NPs. Apparently, the Ge@C/RGO electrode shows a much lower charge-transfer resistance R_{ct} than does the Ge@C electrode (25.7 vs 45.5 Ω) on the basis of the modified Randles equivalent circuit given in the inset of Figure 4d. This result indicates that the Ge@C/RGO electrode possesses a high electrical conductivity, resulting in the better rate capability and higher reversible capacity in comparison with the graphene-free Ge@C NPs, similar to the phenomenon found in many graphene-based hybrids.[21,24]

In conclusion, we have presented a facile method for preparing a Ge@C/RGO nanocomposite, leading to the double protection of Ge NPs through Ge@C core−shell nanostructures and RGO networks. In addition to the preparation of Ge@C NPs, a key to its realization is embedding the NPs wrapped within carbon shells into RGO networks. As an anode material for Li ion batteries, the nanocomposite exhibits excellent cycling performance and rate capability in comparison with pristine Ge@C NPs, which could be attributed to the electronically conductive and elastic RGO networks as well as the carbon shells and the small size of the Ge NPs. This double protection strategy could offer an effective and general approach to improving the cyclability and rate capability of high-capacity electrode materials with large volume variations and low electrical conductivities in the battery area.

■ ASSOCIATED CONTENT

Supporting Information

Preparation of the Ge@C/RGO nanocomposites, TGA of the Ge@C NPs, and discharge−charge voltage profiles of the Ge@C/RGO nanocomposite and Ge@C NPs under different current densities. This material is available free of charge via the Internet at http://pubs.acs.org.

dx.doi.org/10.1021/ja211266m | J. Am. Chem.Soc. 2012, 134, 2512−2515

AUTHOR INFORMATION

Corresponding Author

ygguo@iccas.ac.cn; wanlijun@iccas.ac.cn

ACKNOWLEDGMENTS

This work was supported by the National Basic Research Program of China (Grants 2011CB935700, 2009CB930400, and 2012CB932900), the National Natural Science Foundation of China (Grants 91127044, 21121063, and 50730005), and the Chinese Academy of Sciences.

REFERENCES

(1) Armand, M.; Tarascon, J. M. *Nature* **2008**, *451*, 652.
(2) Wang, B.; Chen, J. S.; Wu, H. B.; Wang, Z.; Lou, X. W. *J. Am. Chem. Soc.* **2011**, *133*, 17146.
(3) Cheng, F.; Liang, J.; Tao, Z.; Chen, J. *Adv. Mater.* **2011**, *23*, 1695.
(4) Cheng, F.; Tao, Z.; Liang, J.; Chen, J. *Chem. Mater.* **2008**, *20*, 667.
(5) Winter, M.; Besenhard, J. O.; Spahr, M. E.; Novák, P. *Adv. Mater.* **1998**, *10*, 725.
(6) Graetz, J.; Ahn, C. C.; Yazami, R.; Fultz, B. *J. Electrochem. Soc.* **2004**, *151*, A698.
(7) Wang, D.; Chang, Y.-L.; Wang, Q.; Cao, J.; Farmer, D. B.; Gordon, R. G.; Dai, H. *J. Am. Chem. Soc.* **2004**, *126*, 11602.
(8) Fuller, C. S.; Severiens, J. C. *Phys. Rev.* **1954**, *96*, 21.
(9) Cui, G.; Gu, L.; Zhi, L.; Kaskhedikar, N.; van Aken, P. A.; Müllen, K.; Maier, J. *Adv. Mater.* **2008**, *20*, 3079.
(10) Lee, H.; Cho, J. *Nano Lett.* **2007**, *7*, 2638.
(11) Lee, H.; Kim, H.; Doo, S.-G.; Cho, J. *J. Electrochem. Soc.* **2007**, *154*, A343.
(12) Chan, C. K.; Zhang, X. F.; Cui, Y. *Nano Lett.* **2008**, *8*, 307.
(13) Seo, M.-H.; Park, M.; Lee, K. T.; Kim, K.; Kim, J.; Cho, J. *Energy Environ. Sci.* **2011**, *4*, 425.
(14) Liu, X. H.; Huang, S.; Picraux, S. T.; Li, J.; Zhu, T.; Huang, J. Y. *Nano Lett.* **2011**, *11*, 3991.
(15) Park, M.-H.; Cho, Y.; Kim, K.; Kim, J.; Liu, M.; Cho, J. *Angew. Chem.* **2011**, *123*, 9821.
(16) Park, M.-H.; Kim, K.; Kim, J.; Cho, J. *Adv. Mater.* **2010**, *22*, 415.
(17) Cui, G.; Gu, L.; Kaskhedikar, N.; van Aken, P. A.; Maier, J. *Electrochim. Acta* **2010**, *55*, 985.
(18) Guo, Y.-G.; Hu, J.-S.; Wan, L.-J. *Adv. Mater.* **2008**, *20*, 2878.
(19) Zhang, L.-S.; Jiang, L.-Y.; Yan, H.-J.; Wang, W. D.; Wang, W.; Song, W.-G.; Guo, Y.-G.; Wan, L.-J. *J. Mater. Chem.* **2010**, *20*, 5462.
(20) Wang, H.; Cui, L.-F.; Yang, Y.; Sanchez Casalongue, H.; Robinson, J. T.; Liang, Y.; Cui, Y.; Dai, H. *J. Am. Chem. Soc.* **2010**, *132*, 13978.
(21) Sun, Y.; Hu, X.; Luo, W.; Huang, Y. *ACS Nano* **2011**, *5*, 7100.
(22) Paek, S.-M.; Yoo, E.; Honma, I. *Nano Lett.* **2009**, *9*, 72.
(23) Guo, W.; Yin, Y.-X.; Xin, S.; Guo, Y.-G.; Wan, L.-J. *Energy Environ. Sci.* **2012**, *5*, 5221.
(24) Yang, S.; Feng, X.; Ivanovici, S.; Müllen, K. *Angew. Chem., Int. Ed.* **2010**, *49*, 8408.
(25) Li, B.; Cao, H.; Shao, J.; Qu, M. *Chem. Commun.* **2011**, *47*, 10374.
(26) Wang, B.; Wu, X.-L.; Shu, C.-Y.; Guo, Y.-G.; Wang, C.-R. *J. Mater. Chem.* **2010**, *20*, 10661.
(27) Ding, S.; Chen, J. S.; Luan, D.; Boey, F. Y. C.; Madhavi, S.; Lou, X. W. *Chem. Commun.* **2011**, *47*, 5780.
(28) Cao, F.-F.; Guo, Y.-G.; Zheng, S.-F.; Wu, X.-L.; Jiang, L.-Y.; Bi, R.-R.; Wan, L.-J.; Maier, J. *Chem. Mater.* **2010**, *22*, 1908.
(29) Cao, F.-F.; Deng, J.-W.; Xin, S.; Ji, H.-X.; Schmidt, O. G.; Wan, L.-J.; Guo, Y.-G. *Adv. Mater.* **2011**, *23*, 4415.
(30) Wu, X.-L.; Jiang, L.-Y.; Cao, F.-F.; Guo, Y.-G.; Wan, L.-J. *Adv. Mater.* **2009**, *21*, 2710.
(31) Zhang, W.-M.; Hu, J.-S.; Guo, Y.-G.; Zheng, S.-F.; Zhong, L.-S.; Song, W.-G.; Wan, L.-J. *Adv. Mater.* **2008**, *20*, 1160.
(32) Wang, X.-L.; Han, W.-Q.; Chen, H.; Bai, J.; Tyson, T. A.; Yu, X.-Q.; Wang, X.-J.; Yang, X.-Q. *J. Am. Chem. Soc.* **2011**, *133*, 20692.
(33) Xue, D.-J.; Wang, J.-J.; Wang, Y.-Q.; Xin, S.; Guo, Y.-G.; Wan, L.-J. *Adv. Mater.* **2011**, *23*, 3704.
(34) Hummers, W. S.; Offeman, R. E. *J. Am. Chem. Soc.* **1958**, *80*, 1339.
(35) Yin, Y.-X.; Xin, S.; Wan, L.-J.; Li, C.-J.; Guo, Y.-G. *J. Phys. Chem. C* **2011**, *115*, 14148.
(36) Hu, Y.-S.; Demir-Cakan, R.; Titirici, M.-M.; Müller, J.-O.; Schlögl, R.; Antonietti, M.; Maier, J. *Angew. Chem., Int. Ed.* **2008**, *47*, 1645.